

NJC

Accepted Manuscript



This is an *Accepted Manuscript*, which has been through the Royal Society of Chemistry peer review process and has been accepted for publication.

Accepted Manuscripts are published online shortly after acceptance, before technical editing, formatting and proof reading. Using this free service, authors can make their results available to the community, in citable form, before we publish the edited article. We will replace this *Accepted Manuscript* with the edited and formatted *Advance Article* as soon as it is available.

You can find more information about *Accepted Manuscripts* in the [Information for Authors](#).

Please note that technical editing may introduce minor changes to the text and/or graphics, which may alter content. The journal's standard [Terms & Conditions](#) and the [Ethical guidelines](#) still apply. In no event shall the Royal Society of Chemistry be held responsible for any errors or omissions in this *Accepted Manuscript* or any consequences arising from the use of any information it contains.



NJC

ARTICLE

Nickel foam supported mesoporous NiCo₂O₄ arrays with excellent methanol electro-oxidation performance

Wei Wang,^a Qingxin Chu,^b Yingnan Zhang,^a Wei Zhu,^a Xiaofeng Wang^a and Xiaoyang Liu^{*a}

Received 00th January 20xx,
Accepted 00th January 20xx

DOI: 10.1039/x0xx00000x

www.rsc.org/

In this paper, nickel foam supported NiCo₂O₄ nanosheet and nanocloth arrays are directly prepared by a mild hydrothermal method and applied to methanol electro-oxidation. Several techniques including powder X-ray diffraction (XRD), scanning electron microscopy (SEM), transmission electron microscopy (TEM), X-ray photoelectron spectra (XPS), Energy-dispersive spectroscopy (EDS) and nitrogen absorption measurements have been employed to characterize the physicochemical properties of as-prepared catalysts. The electrocatalytic performances are investigated by cyclic voltammetry (CV), chronoamperometry (CA) measurements and electrochemical impedance spectroscopy (EIS). Impressively, NiCo₂O₄ nanosheet and nanocloth arrays both deliver excellent electrocatalytic performance for methanol electro-oxidation in alkaline medium, including low onset potential (0.19V, 0.16V), high current densities (111 mA cm⁻², 134 mA cm⁻²) and a desirable electro-oxidation stability (90%, 88%), respectively. The excellent electrocatalytic performances of nickel foam supported NiCo₂O₄ nanosheet and nanocloth arrays originate from their unique 3D mesoporous architecture, which can provide adequate open spaces and shorter ion diffusion paths to facilitate rapid ionic transportation.

Introduction

As fossil fuels approaching depletion and environmental concerns arising intensively, people gradually set their sights on the development of cleaner energy for future demands. Lately, direct methanol fuel cells (DMFCs) as an energy conversion device with high efficiency, high energy density, low-to-zero emission and high performance at low cost, have received enormous attention as the promising next generation power sources. They are considered to be one of the best way to solve the energy problems.^[1-5] Nevertheless, several problems should be taken into consideration, including cost issues, stability and life cycles of the catalysts. As the most commonly and effective catalysts used, the high cost of platinum and its alloys have restrained the commercialization of DMFCs.^[6,7] Therefore, it is necessary to make full use of non-Pt catalysts which can substantially lower the cost of the fuel cell system.

Transition metal oxides, such as Co₃O₄ or NiO, have been considered to be the promising alternative low-cost candidates for DMFCs applications. For instance, NiO/CNTs^[8], Pt-NiO/C^[9], Co₃O₄/NiO^[10], and PdO-Co₃O₄ nanofiber composites^[11] have become the research focus in recent years in the fuel cell community. To the best of our knowledge, their excellent performances are mainly related to the easy ion transportation and the process of rich redox reactions of nickel or cobalt. Consequently, binary metal oxides such as spinel nickel cobaltite (NiCo₂O₄) are expected to be a

more cost-effective material while exhibiting superior electrochemical properties, probably because of the simultaneous existence of the redox reactions of cobalt and nickel ions.^[12] Previously, several significant researches have been devoted to the electrochemical applications of NiCo₂O₄ for supercapacitors,^[12-14] lithium ion batteries,^[15] catalyst materials for oxygen reduction reactions,^[16] and so on. Furthermore, NiCo₂O₄ materials have also shown excellent electro-catalytic activities for methanol electro-oxidation. Currently, different types of nanostructured NiCo₂O₄ have been attempted to construct high-performance DMFCs. For instance, NiCo₂O₄ nanoparticles,^[17] urchin-like hollow structures^[18] and nanosphere-like NiCo₂O₄^[19] have been prepared, which display high electro-catalytic activity and good long-term stability. It appears that the enhanced electrochemical characteristics are primarily evident in the nanostructured NiCo₂O₄ materials, making them promising electrode materials for non-Pt catalysts based DMFCs. However, the methods of fabricating electrodes in most previous reports are traditional preparation processes, which utilize polymer binders and carbon black as conductive agent to avoid the loss of the electroactive species. The polymer binders may set back the kinetics of transmission of electrolytes ions between the electrode and electrolytes, and reduce electrolytes penetration through the active materials. Therefore, it is necessary to design a rational electrode for DMFCs.

Recently, NiCo₂O₄ nanoneedles have been grown on graphene-nickel foam conductive substrate for methanol electro-oxidation, which display high electrocatalytic activity and stability.^[20] However, the fabrication process of graphene-nickel foam is complicated, and the direct use of nickel foam as a substrate to grow different morphologies of active materials is more convenient for methanol electro-oxidation.^[10] In our work, we propose mesoporous NiCo₂O₄ nanosheet and nanocloth arrays directly grown on nickel foam for

^a State Key Laboratory of Inorganic Synthesis and Preparative Chemistry, College of Chemistry, Jilin University, Changchun 130012, P. R. China.

^b Center for High Pressure Science and Technology Advanced Research, Changchun 130012, P. R. China.

E-mail: liuxy@jl.u.edu.cn (Xiaoyang Liu)

Tel: (+86)-0431-85168316.

Electronic Supplementary Information (ESI) available: See

DOI: 10.1039/x0xx00000x

methanol electro-oxidation. They display high electrocatalytic activity and desirable stability.

Experimental

Growing NiCo₂O₄ nanosheet and nanocloth arrays on nickel foam

Nickel foam (approximately 1 cm × 3 cm) was carefully cleaned with 3 M HCl solution in an ultrasound bath for 20 minutes for the sake of removing the NiO layer on the surface, and then rinsed with deionized water and absolute ethanol several times. In a typical synthesis, 1 mmol of Ni(NO₃)₂·6H₂O, 2 mmol of Co(NO₃)₂·6H₂O, 6 mmol of NH₄F and 15 mmol of urea were dissolved in 70 mL and 35 mL of deionized water with magnetic stirring for 30 minutes in the air. After forming a clear pink solution, the reaction mixture was transferred to a 15 mL Teflon-lined stainless-steel autoclave, into which a piece of pretreated nickel foam was immersed. The autoclave was sealed and maintained at 120 °C for 3 h, and then cooled down to room temperature. The obtained precursors were collected and rinsed with deionized water for several times, then dried at 60 °C in air. Subsequently, the precursors were annealed at 320 °C in the air for 2 h with a ramping rate of 1 °C min⁻¹. The resulting precursors on nickel foams were transformed into NiCo₂O₄ nanosheet and nanocloth arrays which were noted as NCO-NS and NCO-NC, respectively.

Material characterizations and electrochemical measurements

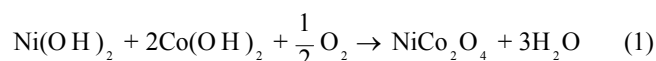
Powder X-ray diffraction (XRD) was recorded on a Rigaku D/MAX 2550 diffractometer with Cu K α radiation ($\lambda=1.5418$ Å). X-ray photoelectron spectra (XPS) with Al-K α radiation at 1486.6 eV (ESCALAB 250 Thermo) was used to investigate the valence states in the synthesized samples. During each scan the C1s peak positioned at 284.6 eV was recorded as the energy reference. Scanning electron microscopy (SEM) images were taken with a JEOL JSM-6700F microscope operating at 10 kV. Transmission electron microscopy (TEM) measurements were made on a CHI H-8100 transmission electron microscope with an accelerating voltage of 200 kV. The specific surface area and pore size distribution of as-prepared catalysts were measured using a BET analyzer (Micromeritics ASAP 2420) at 77 K. Energy-dispersive spectroscopy (EDS) was performed on an Oxford INCA energy-dispersive analyzer. Thermogravimetric analysis (TGA) was conducted with a heating rate of 10 K min⁻¹ using a STA 449C in air. Raman microscopy spectra were recorded using a Renishaw Raman microprobe spectrometer.

All the electrochemical tests were conducted with a CHI 760C electrochemical workstation with a three-electrode cell where Pt plate (1cm × 1cm) served as the counter electrode (CE) and a saturated calomel electrode as the reference electrode (RE), NiCo₂O₄ nanosheet (NCO-NS) and NiCo₂O₄ nanocloth (NCO-NC) arrays were directly used as the working electrode (WE). Cyclic voltammetry (CV) tests were performed at scanning rates of 10 mV s⁻¹ between 0 and 0.6V at room temperature. Chronoamperometry (CA) tests were conducted under the potential of 0.6 V (vs. SCE) for consecutive 1000 s. EIS experiments were taken under open circuit

voltage (OCV) with an ac amplitude of 5 mV over frequency range of 100 kHz -10 mHz. The electrolytes for the tests were 1 M KOH with and without 0.5 M methanol. The equivalent-circuit parameters were analyzed by the software, ZSimpWin.

Results and discussion

Fig. S1 shows the thermogravimetric analysis (TGA) plots for the precursors of NCO-NS and NCO-NC. It can be seen that the TGA plots show three regions of weight loss. The first weight loss below 210 °C can be attributed to the evaporation of chemisorbed water. The second weight loss occurs between 210-400 °C mainly associated to the oxidation of Ni-Co hydroxides and formation of spinel NiCo₂O₄, which can be simply described as follows:



A weight loss was also observed after 400 °C, which can be construed as the decomposition of spinel NiCo₂O₄. In order to prepare more smooth products and avoid the oxidation of nickel foam, it is reasonable to set the low annealing temperature at 320 °C with a slow ramping rate of 1 °C min⁻¹.

XRD analysis had been employed to determine the crystal structure of NCO-NS and NCO-NC. As shown in Fig. 1, the characteristic (111), (220), (311), (222), (511) and (440) crystal planes are clearly evident, except for the three typical peaks originating from the nickel foam. No peaks from other crystallized phases are observed, indicating the presence of high purity phase (JCPDS NO. 20-0781). In addition, the broadened diffraction peaks suggested that poor crystallinity had been obtained, and the size of crystallites should be relatively small.^[21] Fig. S2 shows comparative XRD patterns of the as-obtained NCO-NS and NCO-NC scratched down from nickel foam. It can be seen that all of the diffraction peaks can be indexed to spinel NiCo₂O₄.

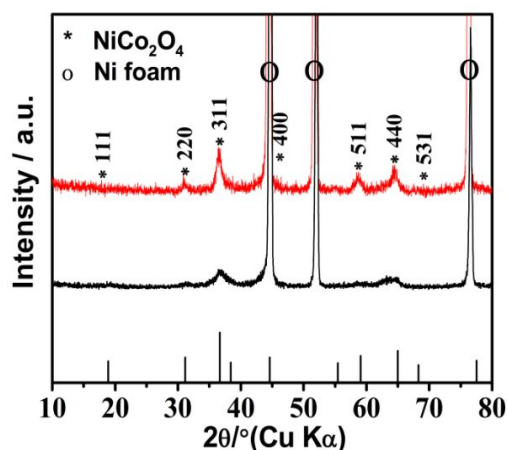


Fig. 1 XRD patterns of NCO-NS (black line); NCO-NC (red line) calcined at 320 °C.

Due to the chemical bonding states of each element of catalysts can affect their catalytic behaviors, XPS analysis on as-prepared catalysts had been conducted, and the typical results of NCO-NC are presented in Fig. 2. It demonstrates that the signals of O 1s, Co 2p

and Ni 2p core levels are detected based on the full scan spectra (Fig. 2A). Specifically, Fig. 2B shows the local XPS spectra of the O 1s region, in which two peaks at 531.3 and 529.4 eV are evident. Presumably, they could be associated with oxygen ions in low coordination sites at the surface and typical metal-oxygen bonds, respectively.^[22] The Co 2p spectra is shown in Fig. 2C, and the peaks at 779.9 eV and 795.6 eV correspond to the Co 2p_{1/2} and Co 2p_{3/2}, respectively, indicating the Co³⁺ ions are dominant in NCO-NC.^[23] Similarly, Ni 2p spectra (Fig. 2D) are composed of Ni 2p_{1/2} (873.4eV) and Ni 2p_{3/2} (856.4eV), which are indexed to Ni²⁺.^[24-25] Meanwhile, the similar Co 2p and Ni 2p spectra of NCO-NS can be also found in Fig. S3. These results show that the surface of both NCO-NC and NCO-NS include the Co³⁺ and Ni²⁺ species, which can provide a large number of active sites for methanol electro-oxidation. It could be one of the imperative factors contributing to the electrocatalytic performance of NiCo₂O₄ materials.^[26] Additionally, the EDX analysis of NCO-NS and NCO-NC (Fig. S4) indicate the presence of Co and Ni species in as-prepared catalysts.

Furthermore, Fig. 4C shows the nanowire-on-nanosheet structure of NCO-NC, which can offer efficient 3D electron transport for oxidation reaction. The HRTEM image of NCO-NC is showed in Fig. 4D, and a d-spacing of 0.25 nm has been determined based on the lattice fringes, which corresponds to the (311) lattice plane of spinel NiCo₂O₄ and agrees well with the result of XRD data. (JCPDS NO. 20-0781).

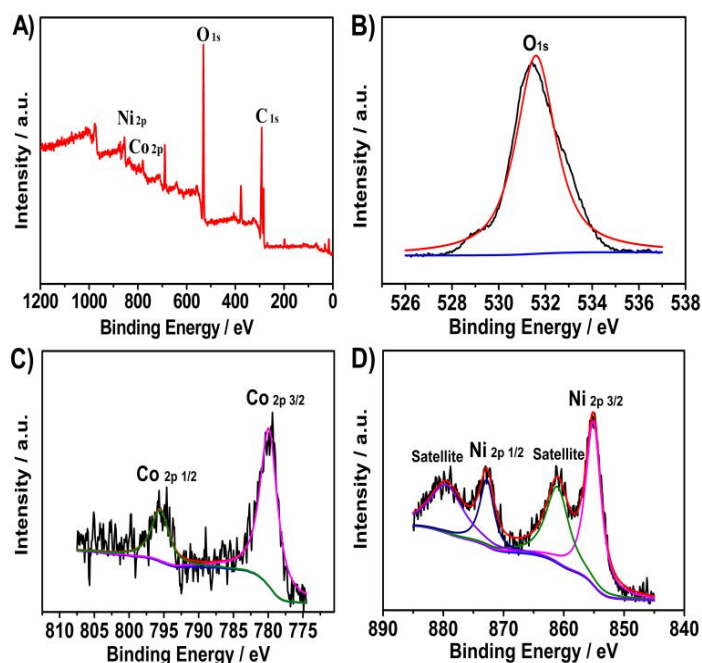


Fig. 2 Survey XPS scan (A); High-resolution XPS spectra of O 1s (B); Co 2p (C) and Ni 2p (D) of NCO-NC.

The morphologies of NCO-NS and NCO-NC are examined by SEM and TEM analysis. As shown in Fig. 3A and B, the obtained nanosheets (NCO-NS) appear to be uniform and smooth, with widths ranging from 0.5 to 1.5 μm . In addition, NCO-NS are almost homogeneously aligned and interconnected with each other. Fig. 3C-D reveal that NCO-NC are also grown uniformly on nickel foam. Moreover, the high-magnification images in Fig. S5 show that nanowires selectively deposit on the surface of nanosheets which are intertwined with each other to afford the cloth-like nanostructure. A typical TEM image of the nanosheets carefully scraped off from nickel foam is presented in Fig. 4A. It exhibits obviously mesopores which are uniformly distributed throughout the nanosheets. The corresponding high-resolution TEM image of NCO-NS (Fig. 4B) reveals a d-spacing of 0.47 nm for the (111) crystal plane.

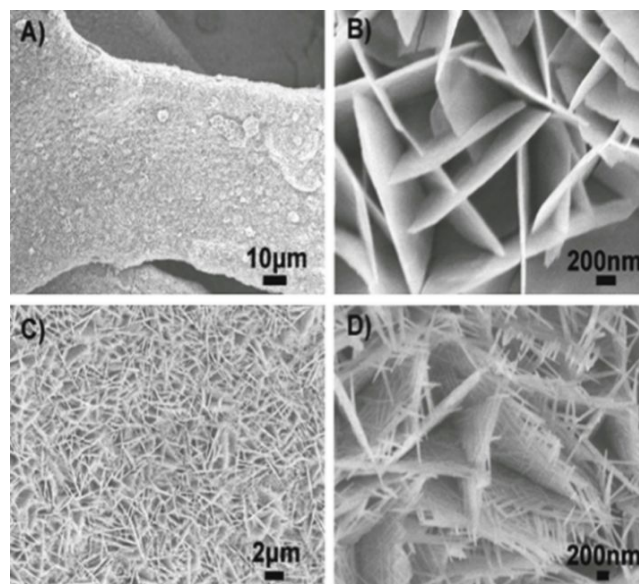


Fig. 3 SEM images of NCO-NS (A-B); NCO-NC (C-D) grown on nickel foam.

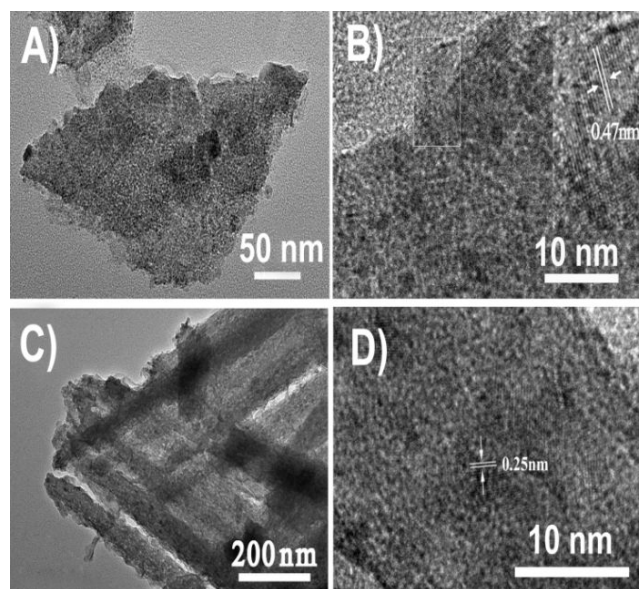


Fig. 4 TEM characterization of (A) NCO-NS; (C) NCO-NC; HRTEM images of (B)NCO-NS; (D) NCO-NC scratched down from nickel foam.

Nitrogen sorption measurements are conducted to evaluate the surface area and porosity properties of as-prepared catalysts. From the Nitrogen adsorption-desorption isotherms in Fig. 5A and 5B, the

hysteresis loops can be distinctly seen, indicating the mesoporous structure of the materials. The corresponding pore size distribution (inset of Fig. 5A and 5B) further confirms the characteristic of mesoporous structure. According to the investigative results, NCO-NC has slightly higher specific surface area ($66.9 \text{ m}^2 \text{ g}^{-1}$) than that of NCO-NS ($54.2 \text{ m}^2 \text{ g}^{-1}$). Moreover, NCO-NC exhibits a narrow pore size distribution around 2.2 nm and a relatively wide pore size distribution around 9.1 nm. Besides, the pore size distribution of NCO-NS mainly centers at 9 nm. The mesoporous structure can afford more active sites and boost electrochemical kinetics during the oxidation reduction process. Therefore, the superior surface structures of NCO-NC are of large benefit for methanol electro-oxidation than that of NCO-NS.

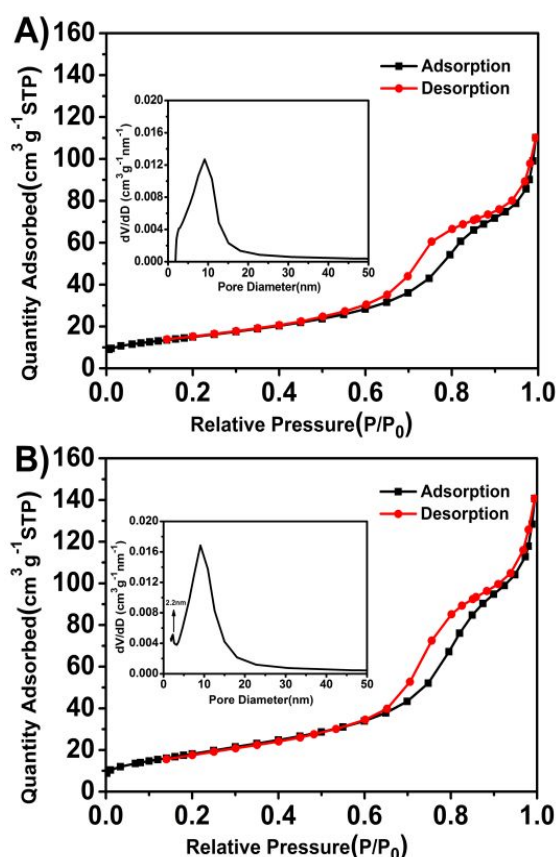
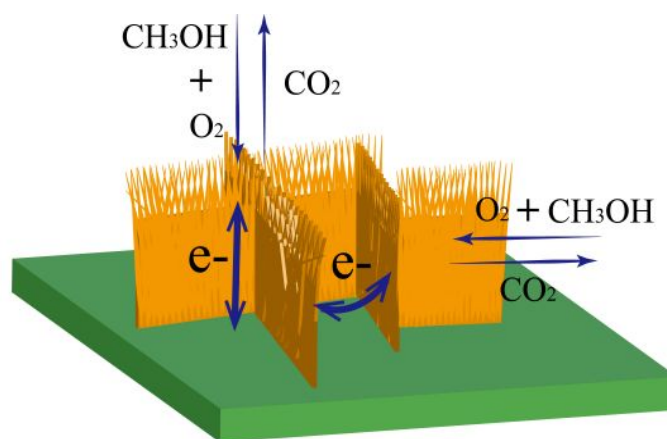
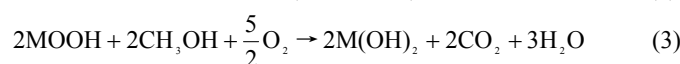
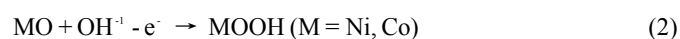


Fig. 5 Nitrogen adsorption–desorption isotherm and the corresponding pore size distribution (inset) of (A) NCO-NS and (B) NCO-NC.

The methanol electro-oxidation performance of NiCo_2O_4 electrodes are initially evaluated by CV, and Co_3O_4 and NiO electrodes prepared by the same methods were used for comparison. Fig. 6A shows the CV plots of NCO-NS and NCO-NC electrodes in 1 M KOH electrolytes from 0 to 0.6 V at a scan rate of 10 mV s^{-1} . It appears that the shapes of the CV plots are consistent with the ones expected for pseudocapacitive processes. The redox peaks originate from the Faradaic reaction relating to the reversible reactions of $\text{Co}^{2+}/\text{Co}^{3+}$ and $\text{Ni}^{2+}/\text{Ni}^{3+}$.^[27-29] Note that, the NCO-NC electrode exhibits a larger enclosed area and broader redox peaks than that of NCO-NS electrode, which means that the former has a higher

electrochemical activity. In order to demonstrate that the NiCo_2O_4 array grown on nickel foam is favorable catalyst for methanol oxidation, the electro-catalytic activities of methanol oxidation on NiO and Co_3O_4 and blank nickel foam electrodes were compared in Fig. 6B. Apparently, NiO and Co_3O_4 and blank nickel foam electrodes show different behavior in 1 M KOH with 0.5 M methanol. By comparing the currents at 0.6V, it is obvious that NiCo_2O_4 electrodes have higher catalytic activity for methanol electro-oxidation than that of other electrodes. In addition, Raman spectra of 1 M KOH electrolytes with 0.5 M methanol after 500 cycles can prove that CH_3OH has been oxidized to other intermediate products (Fig. S9). The current of blank nickel foam is much lower, thus the activity of blank nickel foam for methanol oxidation can be ignored (Fig. S10).^[19] The details of the reaction process can be seen in Scheme 1 and the mechanism of methanol electro-oxidation on each electrode can be simply described as follows:^[30-32]



Scheme 1 The details of the electro-oxidation reaction process of NiCo_2O_4 nanocloth arrays on nickel foam. The unique morphological features can afford efficient 3D electron transport during the redox reaction.

Current density is an important parameter for evaluating the performance of the catalysts. From Fig. 6C and D, it is observed that the maximum current density of NCO-NC electrode can reach 134 mA cm^{-2} at 0.6V, indicating the excellent electrocatalytic activity of NCO-NC for methanol oxidation. The enhanced electrocatalytic performance of NCO-NC is mainly ascribed to its superior mesoporous architecture and unique morphological features than that of NCO-NS (111 mA cm^{-2}). Remarkably, the electro-oxidation performance of NCO-NC is much better than those of NiO/CNTs composites^[8], Pt-NiO/C composites^[9], nickel cobaltite nanoparticles^[17], porous NiCo_2O_4 ^[33], coral-like nickel cobalt oxides^[34]. Furthermore, the onset potential of methanol oxidation on NCO-NC and NCO-NS are about 0.16 V and 0.19 V, respectively, which are much lower than those of reported NiCo_2O_4 electrodes,^[10,17-19, 33,34] The low onset potential and high current density indicate that nickel

foam supported NiCo_2O_4 arrays have excellent performance for methanol electro-oxidation.

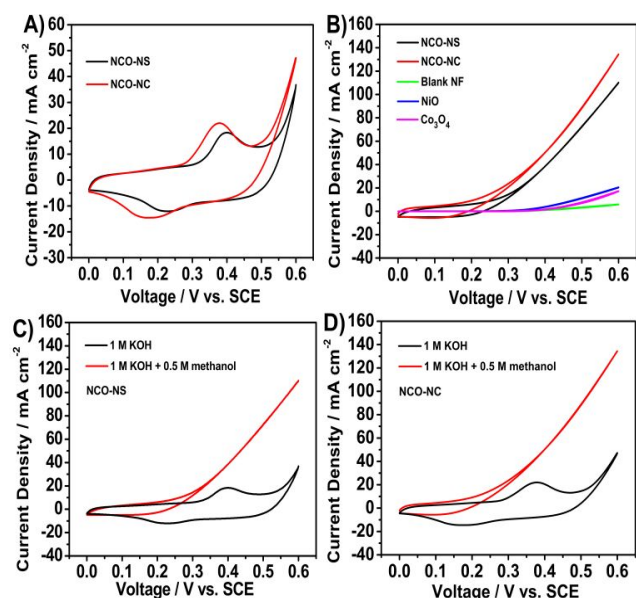


Fig. 6 (A) CV plots of NCO-NS and NCO-NC electrodes in 1 M KOH electrolytes without 0.5 M methanol at a scan rate of 10 mV s^{-1} ; (B) CV plots of NCO-NS, NCO-NC, Co_3O_4 , NiO and nickel foam electrodes in 1 M KOH electrolytes with 0.5 M methanol at a scan rate of 10 mV s^{-1} ; CV plots in 1 M KOH electrolytes without and with 0.5 M methanol for NCO-NS (C) and NCO-NC (D) electrodes at a scan rate of 10 mV s^{-1} respectively.

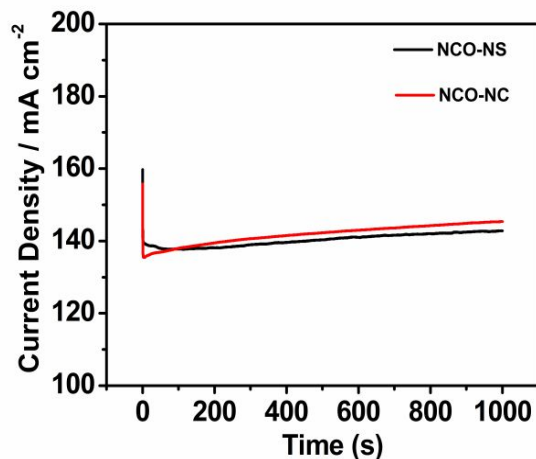


Fig. 7 CA plots in 1 M KOH electrolytes with 0.5 M methanol at 0.6 V (vs. SCE) of as-prepared NCO-NS and NCO-NC electrodes.

In order to investigate the electrochemical stability of the electrocatalysts, the chronoamperometric tests are performed at 0.6 V for consecutive 1000 s. As shown in Fig. 7, it is observed that NCO-NC electrode remains 93% retention based on the initial value, comparing with 89% retention for NCO-NS. Notably, an interesting phenomenon can be seen that the electrolysis current increases steadily, which is due to the activation and wettability occurred on the electrode surface, making the catalysts more active and causing

more electroactive surface areas.^[35, 36] Long-term stability of both electrodes are also examined by CV. Fig. 8A shows that the current density of NCO-NS has 82% retention after 1000 cycles at a rate of 10 mV s^{-1} , comparing with 83% retention for NCO-NC (Fig. 8B). When replacing the new 1 M KOH electrolytes with 0.5 M methanol, the current density of NCO-NS and NCO-NC at 0.6 V can be returned to 90% and 88% of the original value, respectively. It means that the decay of the current density may probably due to the reduction of methanol. Noticeably, after 1000 cycles, the morphologies and structures of both electrodes are well preserved which are depicted in the inset images of Fig. 8A and B, indicating the desirable electrocatalytic stability of the as-prepared catalysts.

The charge transfer (R_{ct}) characteristics and the “knee” frequency (f_{knee}) are important factors affecting the electrocatalytic activity and stability of the catalysts, thus EIS measurements for both electrodes are further investigated in 1 M KOH without and with 0.5 M methanol. The Nyquist plots and admittance plots of experimental and fitting data are shown in Fig. 9A, B and Fig. 9C, D respectively. It is observed that the impedance spectra of NCO-NS and NCO-NC are similar with a semicircle at high frequency region and a straight line at low frequency region, dividing by the “knee” frequency (f_{knee}). In the circuit, R_s , $CPE(Q)$, L , W and R_{ct} represent the solution resistance, the constant phase element corresponding to the double layer capacitance, the inductance, the Warburg impedance and the charge-transfer resistance, respectively.

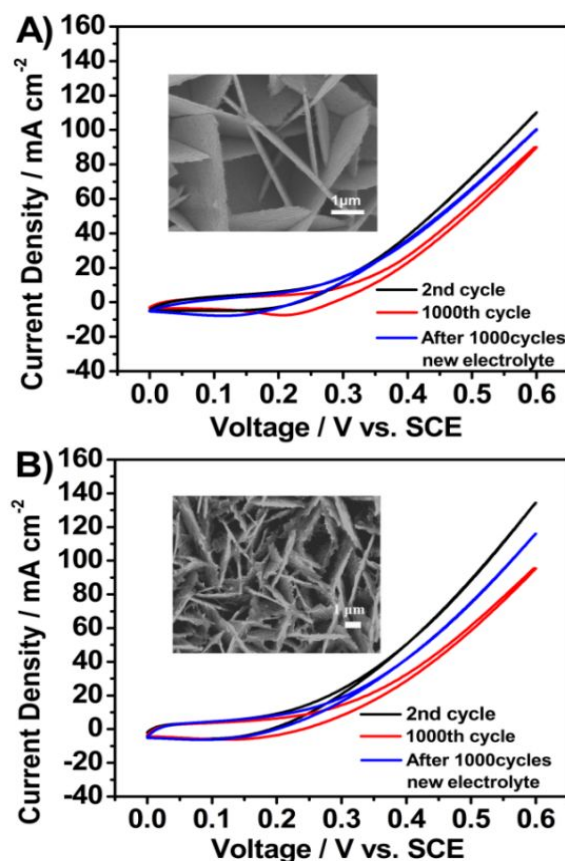


Fig. 8 CV plots of NCO-NS (A) and NCO-NC (B) electrodes in 1 M KOH with 0.5 M methanol measured at a scan rate of 10 mV s^{-1} , the inset images are the SEM images of both electrodes after 1000cycles.

From the inset plots of Fig. 9A, the depressed semicircle of NCO-NC is smaller than that of NCO-NS in the high frequency region, indicating lower R_{ct} between the electrolytes and the active materials [37]. Moreover, when adding methanol into the electrolytes (Fig. 9B), the diameter of the semicircles change slightly before and after addition of methanol, indicating both electrodes have a high tolerance to intermediate poisoning. [38] From the Table 1 in the ESI, in 1 M KOH electrolytes, the NCO-NC electrode exhibits smaller R_{ct} and larger f_{knee} values ($0.89 \Omega \text{ cm}^2$, 31.6 Hz) compared with those ($4.27 \Omega \text{ cm}^2$, 6.8 Hz) of the NCO-NS electrode. In 1 M KOH electrolytes with 0.5 M methanol, the NCO-NC electrode also exhibits smaller R_{ct} and larger f_{knee} values ($0.86 \Omega \text{ cm}^2$, 26.1 Hz) compared with those ($5.02 \Omega \text{ cm}^2$, 2.2 Hz) of the NCO-NS electrode. The results further illustrate that the NCO-NS and NCO-NC based electrodes are both suitable for methanol electro-oxidation and the superior performance of NCO-NC electrode in the catalysis of methanol electro-oxidation.

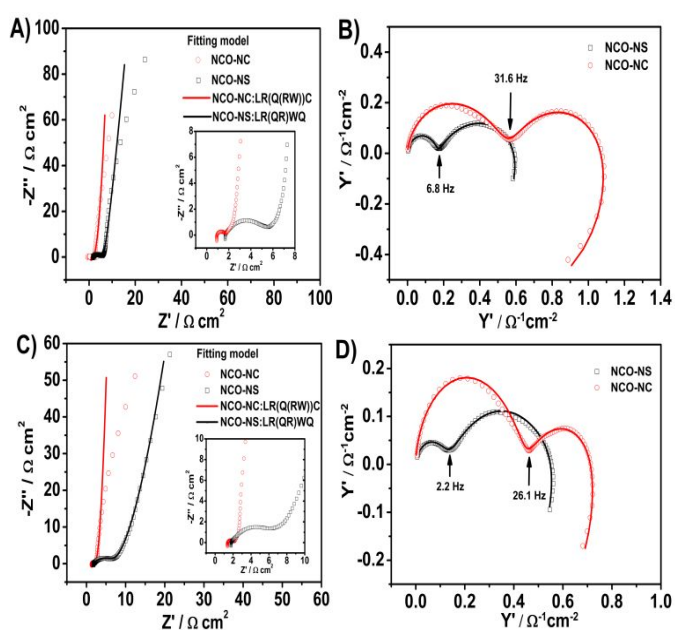


Fig. 9 Nyquist plots (A) and admittance plots (B) in 1 M KOH electrolytes, and Nyquist plots (C) and admittance plots (D) in 1 M KOH electrolytes with 0.5 M methanol of both NiCo_2O_4 electrodes (Inset shows the enlarged parts in the high frequency regions and fitting models, hollow symbols and solid lines represent the experimental and fitting data respectively).

The excellent methanol electro-oxidation property of the mesoporous NCO-NS and NCO-NC could be explained as follows: (1) 3D structure possess structural advantage which allow electrons and ions penetration into the inner space of the electrode, increasing the utilization of the active materials. (2) The mesoporous architecture offer richer active sites, which lead to higher electrochemical performance in the oxidation reactions. (3) The materials directly grown on the nickel foam ensures good mechanical adhesion and electrical connection to the current collector without use of polymer binders and conducting additives. Due to these competitive advantages, nickel foam supported

mesoporous NiCo_2O_4 arrays can exhibit excellent electrochemical performance.

Conclusions

In conclusion, the NiCo_2O_4 nanosheet and nanocloth arrays have been successfully fabricated via a mild method for methanol electro-oxidation. Particularly, both NiCo_2O_4 catalysts exhibit excellent electrochemical performance for methanol electro-oxidation, including low onset potential, high current densities and desirable stability. The remarkable electrocatalytic activities of as-prepared catalysts are ascribed to their superior mesoporous architecture and unique morphological features leading to rapid ionic transportation during the oxidation process. The NCO-NC electrode shows a current density of 134 mA cm^{-2} at 0.6 V and displays a desirable stability with 88% current retention after 1000 cycles. Therefore, it is suggested that nickel foam-support NiCo_2O_4 arrays might be the potential binder-free catalytic electrodes for direct methanol fuel cells.

Acknowledgement

This work is supported by the National Sciences Foundation of China (No.21271082).

Notes and references

- Y. Lu, J. Tu, C. Gu, X. Xia, X. Wang and S. X. Mao, *J. Mater. Chem.*, 2011, **21**, 4843-4849.
- S. K. Kamarudin, F. Achmad and W. R. W. Daud, *Int. J. Hydrogen Energy*, 2009, **34**, 6902-6916.
- T. S. Zhao, R. Chen, W. W. Yang and C. Xu, *J. Power Sources*, 2009, **191**, 185-202.
- M. Z. F. Kamaruddin, S. K. Kamarudin, W. R. W. Daud, M. S. Masdar, *Renew. Sust. Energ. Rev.*, 2013, **24**, 557-565.
- S. Yousefi and M. Zohoor, *Int. J. Hydrogen Energy*, 2014, **39**, 5972-5980.
- C. Koenigsmann and S. S. Wong, *Energy Environ. Sci.*, 2011, **4**, 1161-1176.
- B. Gurau, R. Viswanathan, R. Liu, T. J. Lafrenz, K. L. Ley, E. S. Smotkin, E. Reddington, A. Sapienza, B. C. Chan, T. E. Mallouk and E. S. Smotkini, *J. Phys. Chem. B*, 1998, **102**, 9997-10003.
- X. Tong, Y. Qin, X. Guo, O. Moutanabbir, X. Ao, E. Pippel, L. Zhang and M. Knez, *Small*, 2012, **8**, 3390-3395.
- D. B. Kim, H. J. Chun, Y. K. Lee, H. H. Kwon and H. I. Lee, *Int. J. Hydrogen Energy*, 2010, **35**, 313-320.
- J. B. Wu, Z. G. Li, X. H. Huang and Y. Lin, *J. Power Sources*, 2013, **224**, 1-5.
- Y. Zhang, Y. Wang, J. Jia and J. Wang, *Int. J. Hydrogen Energy*, 2012, **37**, 17947-17953.
- E. Mitchell, A. Jimenez, R. K. Gupta, B. K. Gupta, K. Ramasamy, M. Shahabuddin and S. R. Mishra, *New J. Chem.*, 2015, **39**, 2181-2187.
- W. Zhou, D. Kong, X. Jia, C. Ding, C. Cheng and G. Wen, *J. Mater. Chem. A*, 2014, **2**, 6310-6315.

- 14 R. Zhou, K. Xu, T. Wang, G. He, Q. Liu, X. Liu, Z. Zhang and J. Hu, *J. Mater. Chem. A*, 2013, **1**, 8560-8566.
- 15 X. Yao, C. Zhao, J. Kong, D. Zhou and X. Lu, *RSC Adv.*, 2014, **4**, 37928-37933.
- 16 Y. Xiao, C. Hu, L. Qu, C. Hu and M. Cao, *Chem. Eur. J.*, 2013, **19**, 14271-14278.
- 17 R. Ding, L. Qi, M. Jia and H. Wang, *J. Power Sources*, 2014, **251**, 287-295.
- 18 X. Y. Yu, X. Z. Yao, T. Luo, Y. Jia, J. H. Liu and X. J. Huang, *ACS Appl. Mater. Interfaces*, 2014, **6**, 3689-3695.
- 19 L. Gu, L. Qian, Y. Lei, Y. Wang, J. Li, H. Yuan and D. Xiao, *J. Power Sources*, 2014, **261**, 317-323.
- 20 M. Yu, J. Chen, J. Liu, S. Li, Y. Ma, J. Zhang and J. An, *Electrochim. Acta*, 2015, **151**, 99-108.
- 21 R. Alcántara, M. Jaraba, P. Lavela and J. L. Tirado, *Chem. Mater.*, 2002, **14**, 2847-2848.
- 22 J. F. Marco, J. R. Gancedo, M. Gracia, J. L. Gautier, E. I. Rios, H. M. Palmer, C. Greaves and F. J. Berry, *J. Mater. Chem.*, 2001, **11**, 3087-3093.
- 23 K. Wandelt, *Surf. Sci. Rep.*, 1982, **2**, 1-121.
- 24 Y. E. Roginskaya, O. V. Morozova, E. N. Lubnin, Y. E. Ulitina, G. V. Lopukhova and S. Trasatti, *Langmuir*, 1997, **13**, 4621-4627.
- 25 J. G. Kim, D. L. Pugmire, D. Battaglia, and M. A. Langell, *Appl. Surf. Sci.*, 2000, **165**, 70-84.
- 26 B. Cui, H. Lin, Y. Liu, J. Li, P. Sun, X. Zhao and C. Liu, *J. Phys. Chem. C*, 2009, **113**, 14083-14087.
- 27 G. Hu, C. Tang, C. Li, H. Li, Y. Wang and H. Gong, *J. Electrochem. Soc.*, 2011, **158**, A695-A699.
- 28 V. Gupta, S. Gupta and N. Miura, *J. Power Sources*, 2008, **175**, 680-685.
- 29 X. Wang, X. Han, M. Lim, N. Singh, C. L. Gan, M. Jan and P. S. Lee, *J. Phys. Chem. C*, 2012, **116**, 12448-12454.
- 30 M. Asgari, M. G. Maragheh, R. Davarkhah and E. Lohrasbi, *J. Electrochem. Soc.*, 2011, **158**, K225-K229.
- 31 N. Spinner and W. E. Mustain, *Electrochim. Acta*, 2011, **56**, 5656-5666.
- 32 H. Heli and H. Yadegari, *Electrochim. Acta*, 2010, **55**, 2139-2148.
- 33 R. Ding, L. Qi, M. Jia, and H. Wang, *Electrochim. Acta*, 2013, **113**, 290-301.
- 34 M. Yu, S. Wang, J. Hu, Z. Chen, Y. Bai, L. Wu, J. Chen and X. Weng, *Electrochim. Acta*, 2014, **145**, 300-306.
- 35 F. Lin and S. W. Boettcher, *Nat. Mater.*, 2014, **13**, 81-86.
- 36 F. Švegl, B. Orel, M. G. Hutchins, and K. Kalcher, *J. Electrochem. Soc.*, 1996, **143**, 1532-1539.
- 37 J. Ji, L. L. Zhang, H. Ji, Y. Li, X. Zhao, X. Bai, X. Fan, F. Zhang, R.S. Ruoff, *ACS nano*, 2013, **7**, 6237-6243.
- 38 L. Qian, L. Gu, L. Yang, H. Yuan and D. Xiao, *Nanoscale*, 2013, **5**, 7388-7396.